PERGAMON

International Journal of Heat and Mass Transfer 43 (2000) 3391–3405

International Journal of HEAT and MASS TRANSFER

www.elsevier.com/locate/ijhmt

On the laminar free convection and instability of grade fluids in enclosures

Dennis A. Siginer*, A. Valenzuela-Rendón

Department of Mechanical Engineering, New Jersey Institute of Technology, University Heights, Newark, NJ 07102-1982, USA

Received 23 March 1999; received in revised form 12 November 1999

Abstract

Free convection of rate fluids of the grade type in an inclined cavity of arbitrary aspect ratio is investigated in two dimensions by a regular perturbation in terms of the Grashof number. Fluids of grade N are assumed to be Fourier and Boussinesq fluids. We show that the series are asymptotic in character. Non-Newtonian effects appear at the third order of the analysis even though the Giesekus–Tanner theorem is not valid. The relative contributions of the elastic and shear rate dependent viscosity characteristics of the liquid to the non-Newtonian behavior are investigated through a parametric study, together with the dependence of the Nusselt number on the non-linear properties of the fluid. The effects of the aspect ratio and the inclination of the enclosure on the flow field and the heat transfer coefficient are also investigated. An interesting instability of the fluid of grade three with a negative first Rivlin–Ericksen constant triggered by elastic effects is identified and the implications concerning heat transfer characteristics are discussed.

1. Introduction

Buoyancy driven flows in enclosures are quite common. Well known examples of natural convection of linear fluids are heat transfer across double-glazed windows, solar collectors, electronic cooling, etc. Although these flows are three-dimensional, most studies have solved the two-dimensional equations of motion and energy. However, two-dimensional results provide insight into the more complicated three-dimensional flows. Reviews of the literature for natural convection in rectangular enclosures have been reported by Ostrach [1] and more recently by Gebhart et al. [2].

Many fluids encountered in the food, pharmaceutical, polymer, paper and paint industries exhibit non-Newtonian behavior. Non-isothermal non-Newtonian transport in internal flows is frequently encountered in process industry applications such as flow of polymers, paints, suspensions, etc. in pipes and channels of various configurations. Buoyancy induced effects are undesirable in many of these manufacturing processes. The majority of these flows may fall essentially into the class of forced convection or mixed convection. However, a detailed analysis of pure buoyancy induced convection would give insight into the role and effects of buoyancy in these flows. In spite of its obvious potential importance, there are very few studies, reported in the literature, for free convection in enclosures based on non-Newtonian models. Two recent surveys by Gebhart et al. [2] and Shenoy [3] mention only two studies on natural convection in a rectangular enclosure. One of these concerns viscoinelastic pseudoplastic power law fluids, and reports experimental

* Corresponding author. Tel.: +1-973-596-3331; fax: +1-973-642-4282.

E-mail address: siginer@njit.edu (D.A. Siginer).

0017-9310/00/$ - see front matter
PII: S0017-9310(99)00357-9

Nomenclature

$\underline{A}_i^*$, $i = 1, 2, 3$	the first three Rivlin–Ericksen tensors
C_n, D_n; $-\infty < n < +\infty$	complex constants in the biorthogonal series at the first order of the perturbation algorithm
D	half length of the side of the enclosure parallel to the Y axis
$\underline{e}_X$, $\underline{e}_Y$	unit vectors
E	elasticity number (flow independent): ratio of the Weissenberg and Reynolds numbers
$\epsilon G = Gr$	Grashof number
g	gravitational constant
$G(s)$	shear relaxation modulus
k	power index in the expression for the shear relaxation modulus
l	aspect ratio
L	half length of the side of the enclosure parallel to the X axis
$\overline{Nu}$	average Nusselt number
$Nu(x)$	local Nusselt number
Pr	Prandtl number
Ra	Rayleigh number
Re	Reynolds number
S	shear-thinning number (flow independent): ratio of the secondary shear-thinning number St to the Reynolds number Re
$\underline{S}^*$	dimensional form of the extra-stress tensor
$\underline{S}$	dimensionless form of the extra-stress tensor $\underline{S}^*$
$\underline{S}_i^*$, $i = 1, 2, 3$	dimensional form of the component extra-stress tensors
$\underline{S}_i = \underline{S}^{(j)}$, $i = j = 1, 2, 3$	dimensionless form of the component extra-stress tensors $\underline{S}_i^*$; the superscript (j) indicates order in the perturbation algorithm
s_n, $-\infty < n < +\infty$	complex eigenvalues at the first order of the perturbation algorithm
St	secondary shear-thinning number (flow dependent)
T	dimensional temperature field
T_0	constant low temperature of one side of the enclosure of length $2L$
T_1	constant high temperature of the other side of the enclosure of length $2L$
tr	trace of the second-order tensor
$\underline{u}^* = (u^*, v^*)$	dimensional form of the velocity vector with the X component denoted by u^* and Y component by v^*
W	Weissenberg number
(X, Y)	dimensional coordinates with X and Y axis parallel to the sides of length $2L$ and $2D$, respectively, of the enclosure with the origin situated at mid-point of the box
(x, y)	dimensionless coordinates with x and y axis parallel to the sides of length $2l$ and 2, respectively, of the enclosure with the origin located at mid-point of the box

Greek symbols

α	coefficient of thermal diffusivity
α_i^*, $i = 1, 2$	dimensional Rivlin–Ericksen coefficients (material constants) defined in the limit of zero-shear
α_i, $i = 1, 2$	dimensionless form of the Rivlin–Ericksen coefficients α_i^*
β	coefficient of thermal expansivity
β_i^*, $i = 1, 2, 3$	dimensional material constants of the fluid of grade three defined in the limit of zero-shear
β_i, $i = 1, 2, 3$	dimensionless form of the material constants β_i^* of the fluid of grade three
δ	angle of inclination of the enclosure

ϵ	dimensionless temperature difference between hot and cold walls of length $2l$	θ	dimensionless temperature field
∇^*	dimensional gradient operator	$\theta^{(i)}$, $i = 1, 2, 3$	dimensionless component temperature fields at different orders of the perturbation algorithm
∇	dimensionless form of the gradient operator ∇^*	ρ	density
∇^{*2}	dimensional Laplacian operator	τ	relaxation time
∇^2	dimensionless form of the Laplacian operator ∇^{*2}	$\omega^{(i)}$, $i = 2, 3$	dimensionless component vorticity fields at the second and third orders of the perturbation algorithm
$\phi^* = p - p_0$	dimensional form of the reduced pressure field where p and p_0 are the pressure and the reference pressure, respectively	ψ^*	dimensional form of the stream function
		ψ	dimensionless form of the stream function ψ^*
$\phi_1(n)$, $-\infty < n < +\infty$	complex odd eigenfunctions in the biorthogonal series at the first order of the perturbation algorithm	$\psi^{(i)}$, $i = 1, 2, 3$	dimensionless component stream functions at various orders with the superscript (i) indicating order in the perturbation scheme
Γ	the Gamma function		
μ	zero-shear viscosity	$\frac{\partial(\cdot, \cdot\cdot)}{\partial(x, y)}$	the Wronskian

measurements by Emery et al. [4], and the other by Röpke and Schümmer [5] is a numerical study of the unsteady natural convection of a four parameter Oldroyd fluid.

The wealth of literature concerning the free convection of linear fluids is rather striking when contrasted with the scarcity of corresponding investigations for non-linear fluids. For completeness, we briefly summarize the important developments in the study of the free convection of linear fluids. One of the earliest attempts to solve the problem of the natural convection of Newtonian fluids in a rectangular cavity is the analysis by Batchelor [6] who used a perturbation scheme for small Rayleigh numbers. He concluded that, for a square cavity, conduction is the main mode of heat transfer for $Ra < 1000$. We show that it may not be the case for non-linear fluids. For large Ra, Batchelor's solution leads to a flow with thin boundary layers on the walls and an isothermal core region of constant vorticity. The experimental measurements of Elder [7] and Eckert and Carlson [8] corroborated that conduction is the dominant mode of heat transfer at low Ra. Temperature profile is linear between the vertical walls and the flow field exhibits a single cell with the fluid rising and descending along the hot and cold walls, respectively. At large Ra, thermal and hydrodynamic boundary layers develop on the vertical walls with a thermally stratified and almost stagnant core region. For deep cavities, Gill [9] obtained an approximate solution to the boundary layer equations using a modified Oseen method. Shallow enclosures were investigated analytically by Cormack et al. [10]. They used the method of matched asymptotic expansions to show that in the limit as the aspect ratio goes to zero, i.e. for almost flat enclosures, the temperature distribution is linear and corresponds to pure conduction and the flow in the core region is parallel. From their numerical studies, they also determine the range of validity of their asymptotic expansion. Companion papers by Imberger [11] and Cormack et al. [12] report experimental and numerical results, respectively, in shallow cavities.

Several other numerical studies for vertical square cavities can be found in the literature, for instance, Wilkes and Churchill [13], de Vahl Davis [14], Roux et al. [15] to name a few. These studies solve the coupled energy and momentum equations using the stream function-vorticity formulation by means of different finite difference schemes. Studies of natural convection in inclined cavities have been reported by Ozoe et al. [16,17]. They performed numerical and experimental studies and determined that the preferred mode of circulation changed with aspect ratio and angle of inclination, and found both numerically and experimentally that maximum heat transfer occurred when the enclosure of aspect ratio one heated from below was inclined at about 50° from the horizontal for values of the Rayleigh number less than 10^4. In the

same parameter range, there is also a local minimum for the heat transfer when the enclosure of aspect ratio one heated from below is about 5° of inclination, [16]. This minimum occurs because heat transfer due to Rayleigh–Bénard type thermal instabilities when the box is horizontal is gradually reduced due to the creeping motion set by gravitational effects as the angle of inclination is increased from 0 to 5°. For inclinations larger than 5°, thermal instabilities are not the dominant mechanism any more and heat transfer increases with increasing angle of inclination up to 50° to decrease thereafter when Rayleigh number is less than 10^4. At higher Rayleigh numbers, maximum heat transfer occurs at 0° for all aspect ratios when heating from below (Arnold et al. [18]). But, the local minimum which was at about 5° for $Ra < 10^4$ and aspect ratio one gradually shifts towards 90° with growing aspect ratios at the same Ra [18]. It appears that the location of the minimum Nusselt number also shifts towards 90° with increasing Ra at fixed aspect ratio. When heating is from above, maximum heat transfer always occurs when constant temperature walls are vertical corresponding to 90° inclination of the enclosure, regardless of the aspect ratio. In this mode, heat transfer at any inclination can be deduced from that at 90° by using scaling laws when Ra is sufficiently large and a boundary layer regime develops, and also when Ra is not large enough to allow essentially a boundary layer flow to result. None of the features of the corresponding behavior of viscoelastic liquids has been studied. We only know that the onset of instability is far more complicated than the Newtonian case, and that although overstability is a distinct theoretical possibility, it may not be observable as very high temperature gradients or large gravity fields are required (Sokolov and Tanner [19]).

This paper is part of a much broader program in which we also study numerically the free convection of the Oldroyd family of fluids with and without zero retardation time such as various Maxwell fluids. In this work, we use grade fluids to study natural convection in a two-dimensional rectangular enclosure. In general, the choice of this rate type constitutive structure would give realistic results in motions with small strain rates. In free convection, although the strains may be large, strain rates are relatively small. In most buoyancy driven motions, the flow is also slow due to moderate temperature gradients. In principle, the constitutive equation of the grade fluids is ideally suited for the study of this class of motions as it comes out of a more general constitutive structure by retarding the flow. We assume that grade fluids are also Fourier and Boussinesq fluids. Presumably, although some viscoelastic fluids are also Boussinesq fluids, not all viscoelastic fluids are necessarily Boussinesq fluids. There is no work towards a proper thermodynamic theory in this area in the literature. But, it has long been assumed that Boussinesq approximation holds for viscoinelastic fluids [2]. This assumption has been extended to cover also viscoelastic fluids starting with Sokolov and Tanner [19], and all the studies reported in the literature use the Boussinesq approximation for both inelastic and elastic fluids.

A perturbation method in terms of the Grashof number is used and the analysis is developed up to and including third and fourth orders, respectively, for the velocity and temperature fields. Dissipation is neglected in the energy equation due to moderate temperature gradients, generating small strain rates and fluid properties are evaluated at an average temperature. We show that the series holds in an asymptotic sense, so that qualitative field descriptions can be obtained for much larger values of the Grashof number than may be allowed for a uniformly convergent series. The fluids of grade two and three naturally arise at the second and third orders of the analysis. Even though the analysis is not taken any further than the third order for the flow field, where non-linear effects appear for the first time, we do not consider the constitutive equation of the fluid of third grade a constitutive equation in its own right, although it is properly frame invariant and meets all the requirements from a continuum mechanics perspective. We rather assume that it is the truncated form of a more general constitutive structure given as an infinite series, and feel that this approach provides enough support to use experimentally determined negative values of the first Rivlin–Ericksen constant.

Fosdick and Rajagopal [20] have shown that for an incompressible liquid of third grade defined by Eqs. (2) and (3), one must have,

$$\mu \geq 0, \quad \alpha_1^* \geq 0, \quad |\alpha_1^* + \alpha_2^*| \leq \sqrt{24\mu\beta_3^*}, \quad \beta_1^* = \beta_2^* = 0, \quad \beta_3^* \geq 0, \tag{1}$$

for good stability characteristics if the fluid of grade three is viewed as a constitutive equation in its own right, assuming that Helmholtz free energy is a minimum in equilibrium and observing the restrictions imposed by the Clausius–Duhem inequality. But, available experimental evidence indicates that $\alpha_1^* < 0$ for the liquids used in these experiments. One may then conjecture that either these fluids are not grade fluids or they abide by a more encompassing constitutive equation of which the fluid of grade three is the truncated form. The latter may lead to relaxing further the condition of positive semi-definiteness $(1)_2$ imposed on the first Rivlin–Ericksen constant. This intuitively deduced trend finds some adhoc support in that if the fluid of second grade is considered to be a constitutive equation in its own right, the first Rivlin–Ericksen con-

stant must be strictly positive for good stability characteristics in view of the thermodynamic restrictions. Some evidence for this view is also provided by the fact that the structure of the fluid of grade three naturally arises at the third-order of any perturbation analysis.

Overall flow patterns in viscoelastic transport resemble qualitatively those in linear fluids, but the velocity levels may be markedly different. The first-order problems for the temperature and velocity fields in this analysis which apply equally well to both Newtonian and non-linear liquids are solved analytically. The temperature field at the first order corresponds to pure conduction. Corrections to this base state describing convective effects are obtained up to and including the fourth order in the perturbation parameter. The field equations of the fluid of grade two emerge at the second order. Although the liquid is incompressible, body forces, i.e. buoyant forces do not have a potential and Giesekus–Tanner theorem does not apply. That is, in general, the flow field of a fluid of grade two is not the same as that of a linear fluid of the same viscosity in non-isothermal flows. But, it turns out that in the problem under consideration here, non-linear terms coming from the extra stress at the second order cancel out, and the flow field is the same as that of the Newtonian fluid of the same viscosity at the second order. The temperature and velocity fields are solved analytically and numerically, respectively, at this order. The solution to the third order flow problem has components representing the Newtonian field and the elastic and shear-thinning effects. Through a parametric study of the relative influence of elasticity and shear rate dependent viscosity in shaping the flow field, we determine that elastic effects are the dominant ones by far. Shear-thinning effects are much smaller than elastic effects at any aspect ratio and angle of inclination. For shallow enclosures, the influence of shear-thinning properties is negligible.

The dependence of the Nusselt number on the flow characteristics is extensively studied. Nusselt number increases with increasing second normal stress effects represented by a dimensionless Elasticity number at fixed Grashof and Prandtl numbers and at any aspect ratio and angle of inclination. It also increases with increasing angle of inclination in the range of Grashof numbers studied when the Elasticity number and the remaining parameters are held fixed. Shear thinning has minimal effect, if at all, on the Nusselt number.

We determine that with $\alpha_1^* < 0$ the flow field of the fluid of grade three either undergoes a loss of evolution or more likely an exchange of stability for a critical value of the Grashof number or equivalently for a critical Elasticity number when the remaining parameters are held fixed. An exchange of stability occurs for gradually smaller critical values of these parameters as the aspect ratio becomes larger at a given angle of inclination. A larger angle of inclination precipitates the onset of this loss of stability. Stability bounds in terms of the Grashof and Elasticity numbers are not given because a stability analysis is not conducted. The perturbation analysis provides a limited window on the stability parameter space. Nevertheless, it is enough to state that the fluid of grade three with $\alpha_1^* < 0$ may be subject to loss of stability in non-isothermal flows.

2. Mathematical formulation

We consider the flow regime in a two-dimensional rectangular cavity of height $2L$ and width $2D$ shown in Fig. 1. The two end walls are kept at different temperatures $T_1 > T_0$ and the remaining walls are insulated.

The governing equations subject to the Boussinesq approximation are,

$$\underline{u}^* \cdot \nabla^* T = \alpha \nabla^{*2} T, \quad \nabla^* \cdot \underline{u}^* = 0,$$

$$\rho \underline{u}^* \cdot \nabla^* \underline{u}^* = -\nabla^* \phi^* + \rho g \beta \left(\underline{e}_X \sin\delta + \underline{e}_Y \cos\delta\right)(T - T_0) + \nabla^* \cdot \underline{S}^*,$$

where $\underline{S}^*$ is the extra stress and ϕ^* is the reduced pressure field, $\phi^* = p - p_0$, p_0 is the static pressure. ρ, β, and α are the density, and the coefficients of thermal expansivity and thermal diffusivity, respectively, all evaluated at some average temperature. The corresponding boundary conditions are:

$$\underline{u}^*(X, \pm D) = \underline{u}^*(\pm L, Y) = 0,$$

$$T(X, D) = T_1, \quad T(X, -D) = T_0, \quad T_{,X}(\pm L, Y) = 0.$$

The extra stress is represented by the series

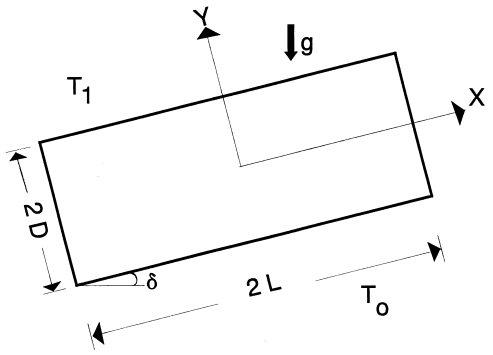

Fig. 1. Flow configuration.

$$\underline{S}^* = \sum_i \underline{S}_i^*, \quad \underline{S}_1^* = \mu \underline{A}_1^*, \quad \underline{S}_2^* = \alpha_1^* \underline{A}_2^* + \alpha_2^* \underline{A}_1^{*^2}, \tag{2}$$

$$\underline{S}_3^* = \beta_1^* \underline{A}_3^* + \beta_2^* \left(\underline{A}_2^* \underline{A}_1^* + \underline{A}_1^* \underline{A}_2^*\right) + \beta_3^* \left(\mathrm{tr}\, \underline{A}_2^*\right) \underline{A}_1^*, \tag{3}$$

where $\underline{A}_n^*$ is the Rivlin–Ericksen tensor of order n given by,

$$\underline{A}_{n+1}^* = \left(\nabla^* A_n^*\right) \underline{u}^* + \underline{A}_n^* \nabla^* \underline{u}^* + \left(\nabla^* \underline{u}^*\right)^{\mathrm{T}} \underline{A}_n^*,$$

$$\underline{A}_1^* = \nabla^* \underline{u}^* + \left(\nabla^* \underline{u}^*\right)^{\mathrm{T}}.$$

μ is the zero-shear viscosity and α_1^*, α_2^*, β_1^*, β_2^*, β_3^* are material constants defined in the limit of zero shear. A stream function ψ^* is introduced,

$$u^* = \psi_{,Y}^*, \quad v^* = \psi_{,X}^*,$$

together with the following definitions,

$$x = \frac{X}{D}, \quad y = \frac{Y}{D}, \quad l = \frac{L}{D}, \quad \theta = \frac{T - T_0}{T_0}, \quad \psi = \frac{\rho}{\mu} \psi^*, \tag{4}$$

to reduce the governing equations to,

$$\nabla^2 \theta = Pr\left(\psi_{,y} \theta_{,x} - \psi_{,x} \theta_{,y}\right), \tag{5}$$

$$\psi_{,x} \nabla^2 \psi_{,y} - \psi_{,y} \nabla^2 \psi_{,x} = G\left(\cos \delta\, \theta_{,x} - \sin \delta\, \theta_{,y}\right) - \nabla \wedge \nabla \cdot \underline{S}, \tag{6}$$

with boundary conditions,

$$\psi_{,x}(\pm l, y) = \psi_{,y}(x, \pm 1) = \psi(\pm l, y) = \psi(x, \pm 1) = 0, \tag{7}$$

$$\theta(x, -1) = 0, \quad \theta(x, 1) = \epsilon, \quad \theta_{,x}(\pm l, y) = 0. \tag{8}$$

In Eqs. (5) and (6), ∇^2 and ∇ are dimensionless operators, $\underline{S}$ is the dimensionless extra stress tensor and $G = \rho^2 g \beta T_0 D^3 / \mu^2$, $Pr = \mu / \rho \alpha$ are dimensionless numbers. The former multiplied with ϵ gives the Grashof number Gr and the latter is the Prandtl number. We now consider a solution to Eqs. (5)–(8) by means of a series expansion of ψ, θ and $\underline{S}$ to linearize both constitutive and inertial non-linearities.

$$\langle \cdot \rangle = \sum_{n=1} \frac{\epsilon^n}{n!} \langle \cdot \rangle^{(n)}, \quad \langle \cdot \rangle^{(n)} = \frac{\partial^n \langle \cdot \rangle}{\partial \epsilon}|_{\epsilon = 0} \tag{9}$$

2.1. First-order solution

First-order problem is obtained from Eqs. (5), (6) and (9),

$$\nabla^2 \theta^{(1)} = 0, \quad \nabla \wedge \nabla \cdot \underline{S}^{(1)} = G\left(\cos \delta\, \theta_{,x}^{(1)} - \sin \delta\, \theta_{,y}^{(1)}\right), \tag{10}$$

with boundary conditions,

$$\theta^{(1)}(x, -1) = 0, \quad \theta^{(1)}(x, 1) = 1, \quad \theta_{,x}^{(1)}(\pm \ell, y) = 0, \tag{11}$$

$$\psi_{,x}^{(1)}(\pm \ell, y) = \psi_{,y}^{(1)}(x, \pm 1) = \psi^{(1)}(\pm \ell, y) = \psi^{(1)}(x, \pm 1) = 0. \tag{12}$$

The solution to the energy equation $(10)_1$ subject to Eq. (11) is given by,

$$\theta^{(1)} = \frac{1}{2}(y + 1), \tag{13}$$

which corresponds to pure conduction. We compute for the first-order momentum balance $(10)_2$,

$$\nabla \wedge \nabla \cdot \underline{S}^{(1)} = \nabla^4 \psi^{(1)} = -\frac{1}{2} G \sin \delta, \quad \psi^{(1)} = G \sin \delta\, \psi_1^{(1)}, \quad \nabla^4 \psi_1^{(1)} = -\frac{1}{2}. \tag{14}$$

An equivalent problem is formulated by transferring the driving term in Eq. $(14)_3$ to the boundary,

$$\nabla^4 \psi_h^{(1)} = 0, \quad \psi_h^{(1)} = \psi^{(1)} - \psi_p^{(1)}, \quad \psi_p^{(1)} = -\frac{\left(y^2 - 1\right)^2}{48},$$

$$\psi_{h,x}^{(1)}(\pm l, y) = \psi_{h,y}^{(1)}(x, \pm 1) = \psi_h^{(1)}(x, \pm 1) = 0.$$

This problem is solved by means of complex biorthogonal series,

$$\psi_h^{(1)} = \sum_{n=-\infty}^{\infty} \frac{C_n \mathrm{e}^{s_n x} + D_n \mathrm{e}^{-s_n x}}{s_n^2} \phi_1^{(n)}(y),$$

$$\phi_1^{(n)} = s_n \sin s_n \cos(s_n y) - s_n y \cos s_n \sin(s_n y), \quad \sin 2s_n + 2s_n = 0,$$

where $\phi_1^{(n)}$ and s_n are complex odd eigenfunctions and complex eigenvalues, respectively. Application of the boundary conditions at $y = \pm 1$ together with biorthogonality yield the following set of algebraic equations to determine the complex constants C_n and D_n,

$$\frac{2}{s_m^2} = \left(C_m \mathrm{e}^{\pm s_m l} + D_m \mathrm{e}^{\pm s_m l}\right) k_m$$

$$+\sum_{-\infty}^{+\infty}\left[C_n e^{\pm s_m l}-\left(\frac{1+s_n}{1-s_n}\right)D_n e^{\pm s_n l}\right]$$

$$\times\left(\frac{1-s_n}{s_n}\right)\int_{-1}^{1}\Psi_2^{(m)}\phi_1^{(n)}\,dy,$$

where

$$\Psi_2^{(m)}=s_m\sin s_m\cos s_m y-s_m y\cos s_m\sin s_m y,$$

$$k_m=-4\cos^2 s_m.$$

Note that $\bar{C}_n=C_{-n}$ and $\bar{D}_n=D_{-n}$. The infinite sums are truncated to N terms to obtain $2N$ equations with $2N$ unknowns for C_n and D_n. The complete solution to Eq. $(10)_2$ is given by,

$$\psi^{(1)}=G\sin\beta\left[\psi_h^{(1)}-\frac{\left(y^2-1\right)^2}{48}\right], \tag{15}$$

which represents a single cell flow rising and descending along the hot and cold walls, respectively.

2.2. Second-order solution

The non-dimensionalized field equations at this order read,

$$\nabla^2\theta^{(2)}=2Pr\left(\psi_{,y}^{(1)}\theta_{,x}^{(1)}-\psi_{,x}^{(1)}\theta_{,y}^{(1)}\right),$$

$$2\left(\psi_{,x}^{(1)}\nabla^2\psi_{,y}^{(1)}-\psi_{,y}^{(1)}\nabla^2\psi_{,x}^{(1)}\right)$$

$$=G\left(\cos\delta\,\theta_{,x}^{(2)}-\sin\delta\,\theta_{,y}^{(2)}\right)+2\nabla\wedge\nabla\cdot\underline{S}^{(2)},$$

with homogeneous boundary conditions. We compute,

$$\nabla\wedge\nabla\cdot\underline{S}^{(2)}=-\frac{1}{2}\nabla^4\psi^{(2)}+\alpha_1\left(\psi_{,x}^{(1)}\nabla^4\psi_{,y}^{(1)}-\psi_{,y}^{(1)}\nabla^4\psi_{,x}^{(1)}\right), \tag{16}$$

$$\alpha_1=\alpha_1^*/\rho D^2.$$

Using Eqs. (13) and $(14)_1$, the field equations at this order can be rewritten as,

$$\nabla^2\theta^{(2)}=Pr\,G\sin\delta\,\psi_{1,y}^{(1)}, \tag{17}$$

$$\nabla^4\psi^{(2)}=G\left(\cos\delta\,\theta_{,x}^{(2)}-\sin\delta\,\theta_{,y}^{(2)}\right)-2\left(\psi_{,x}^{(1)}\nabla^2\psi_{,y}^{(1)}-\psi_{,y}^{(1)}\nabla^2\psi_{,x}^{(1)}\right). \tag{18}$$

The energy equation (17) is solved analytically,

$$\theta^{(2)}=G\,Pr\sin\delta\,\theta_1^{(2)}, \tag{19}$$

$$\theta_1^{(2)}=a_0+\sum_{i=1}^{\infty}a_i\left(e^{\lambda_i x}+e^{-\lambda_i x}\right)\sin\lambda_i y+\sum_{i=1}^{\infty}\left(b_i e^{\gamma_i y}+c_i e^{-\gamma_i y}\right)\cos\gamma_i y+\sum_{n=-\infty}^{\infty}\frac{C_n e^{s_n x}-D_n e^{-s_n x}}{4s_n}$$

$$\times\left[\left(\sin s_n-\frac{\cos s_n}{2s_n}\right)y\sin(s_n y)+\frac{\cos s_n}{2}y^2\cos(s_n y)\right].$$

The parameters in this expression are defined below:

$$a_0=-\frac{1}{8l}\sum_{n-=\infty}^{\infty}\frac{1}{s_n^2}\left(\sin^2 s_n+2\right)(C_n-D_n)\left(e^{s_n l}-e^{-s_n l}\right),$$

$$a_m=-\frac{1}{4l\left(e^{\lambda_m}+e^{-\lambda_m}\right)}\sum_{n=-\infty}^{\infty}\times\frac{\left(\sin^2 s_n+2\right)(C_n+D_n)\left(e^{s_n l}+e^{-s_n l}\right)\sin\lambda_m l}{s_n^2+\lambda_m^2},$$

$$b_m=-\frac{e^{\gamma_m l}F_1-e^{\gamma_m l}F_2}{e^{-2\gamma_m l}-e^{2\gamma_m l}},\quad c_m=-\frac{e^{\gamma_m l}F_1+e^{\gamma_m l}F_2}{e^{-2\gamma_m l}-e^{2\gamma_m l}},$$

$$\lambda_m=\frac{(2m-1)\pi}{2l},\quad \gamma_m=l\lambda_m;\quad m=1,2,\ldots,\infty,$$

$$F_1=\int_{-1}^{1}\theta_{p,x}^{(2)}(l,y)\cos\gamma_m y\,dy,$$

$$F_2=\int_{-1}^{1}\theta_{p,x}^{(2)}(-l,y)\cos\gamma_m y\,dy,$$

$$\theta_p^{(2)}=\sum_{\infty}^{-\infty}\frac{C_n e^{s_n x}-D_n e^{-s_n x}}{2s_n}\left[\left(\sin s_n-\frac{\cos s_n}{2s_n}\right)y\sin s_n y+\frac{\cos s_n}{2}y^2\cos(s_n y)\right].$$

The aspect ratio l is defined in Eq. $(4)_3$, and C_n, D_n and s_n are first-order quantities. Substitution of Eq. (19) into Eq. (18) yields,

$$\nabla^4\psi^{(2)}=G^2 Pr\sin\delta\left(\cos\delta\,\theta_{1,x}^{(2)}-\sin\delta\,\theta_{1,y}^{(1)}\right)-2G^2\sin^2\delta\left(\psi_{1,x}^{(1)}\nabla^2\psi_{1,y}^{(1)}-\psi_{1,y}^{(1)}\nabla^2\psi_{1,x}^{(1)}\right). \tag{20}$$

Introducing the vorticity $\omega=-\nabla^2\psi$ and defining,

$$\psi^{(2)}=G^2 Pr\sin\delta\cos\delta\,\psi_1^{(2)}+G^2\sin^2\delta\left(Pr\psi_2^{(2)}+\psi_3^{(2)}\right), \tag{21}$$

we obtain from Eq. (20) three sets of equations with homogeneous boundary conditions,

$$\nabla^2\omega_1^{(2)} = \theta_{1,x}^{(2)}, \quad \nabla^2\omega_2^{(2)} = -\theta_{1,y}^{(2)},$$

$$\nabla^2\omega_3^{(2)} = -2\left(\omega_{1,x}^{(1)}\psi_{1,y}^{(1)} - \omega_{1,y}^{(1)}\psi_{1,x}^{(1)}\right), \quad \nabla\psi_j^{(2)} = -\omega_j^{(2)};$$

$j = 1, 2, 3.$

The finite difference solution to this set is obtained by optimal successive over-relaxation.

2.3. Third-order solution

The dimensionless field equations at the third order derived from Eqs. (5), (6) and (9) are:

$$\nabla^2\theta^{(3)} = 3Pr\left(\psi_{,y}^{(2)}\theta_{,x}^{(1)} + \psi_{,y}^{(1)}\theta_{,x}^{(2)} - \psi_{,x}^{(2)}\theta_{,y}^{(1)} - \psi_{,x}^{(1)}\theta_{,y}^{(2)}\right), \tag{22}$$

$$\begin{aligned} &3\left(\psi_{,x}^{(2)}\nabla^2\psi_{,y}^{(1)} + \psi_{,x}^{(1)}\nabla^2\psi_{,y}^{(2)} - \psi_{,y}^{(2)}\nabla^2\psi_{,x}^{(1)}\right. \\ &\left. - \psi_{,y}^{(1)}\nabla^2\psi_{,x}^{(2)}\right) \\ &= G\left(\cos\delta\,\theta_{,x}^{(3)} - \sin\delta\,\theta_{,y}^{(3)}\right) + 6\nabla\wedge\nabla\cdot\underline{S}^{(3)} \end{aligned} \tag{23}$$

where

$$\begin{aligned} \nabla\wedge\nabla\cdot\underline{S}^{(3)} = &-\frac{1}{6}\nabla^4\psi^{(3)} + \frac{1}{2}\alpha_1\left(\psi_{,x}^{(1)}\nabla^4\psi_{,y}^{(2)} + \psi_{,x}^{(2)}\nabla^4\psi_{,y}^{(1)}\right. \\ &\left. - \psi_{,y}^{(1)}\nabla^4\psi_{,x}^{(2)} - \psi_{,y}^{(2)}\nabla^4\psi_{,x}^{(1)}\right) + \beta_1\nabla\wedge\nabla \\ &\cdot\underline{A}_3^{(3)} + (\beta_2+\beta_3)\nabla\wedge\nabla\cdot\left[\mathrm{tr}\left(\underline{A}_1^{(1)}\right)^2\right]\underline{A}_1^{(1)}, \end{aligned}$$

$$\beta_1 = \beta_1^*\mu/\rho^2D^4, \quad \beta_2+\beta_3 = \left(\beta_2^*+\beta_3^*\right)\mu/\rho^2D^4. \tag{24}$$

β_i represent dimensionless constitutive constants. The dimensionless first Rivlin–Ericksen constant α_1 was defined in Eq. $(16)_2$. The dimensional counterparts α_1^* and β_i^* appeared in the constitutive structures (2) and (3), respectively. Using Eqs. $(14)_2$ and (21), the energy equation (22) can be recast as,

$$\begin{aligned} \nabla^2\theta^{(3)} = 3Pr\,G^{\,2}\sin\delta\Big[&-\frac{1}{2}\Big(Pr\cos\delta\,\psi_{1,x}^{(2)} \\ &+ Pr\sin\delta\,\psi_{2,x}^{(2)} + \sin\delta\psi_{3,x}^{(2)}\Big) \\ &+ Pr\sin\delta\left(\theta_{1,x}^{(2)}\psi_{1,y}^{(1)} - \theta_{1,y}^{(2)}\psi_{1,x}^{(1)}\right)\Big]. \end{aligned} \tag{25}$$

Defining,

$$\begin{aligned} \theta^{(3)} = &Pr^2G^{\,2}\sin\delta\left(\cos\delta\,\theta_1^{(3)} + \sin\delta\,\theta_2^{(3)}\right) \\ &+ Pr\,G^{\,2}\sin^2\delta\,\theta_3^{(3)}, \end{aligned}$$

we obtain a set of three equations from Eq. (25) for the temperature field,

$$\nabla^2\theta_1^{(3)} = -\frac{3}{2}\psi_{1,x}^{(2)}, \quad \nabla^2\theta_2^{(3)} = -\frac{3}{2}\psi_{2,x}^{(2)} + 3\frac{\partial\left(\theta_1^{(2)},\psi_1^{(1)}\right)}{\partial(x,y)},$$

$$\nabla^2\theta_3^{(2)} = 3\psi_{3,x}^{(2)},$$

all with homogeneous boundary conditions. Similarly, by introducing the vorticity and defining,

$$\begin{aligned} \psi^{(3)} = G^{\,3}\Big[&Pr^2\sin\delta\cos\delta\,\psi_1^{(3)} + Pr^2\sin^2\delta\cos\delta\,\psi_2^{(3)} \\ &+ Pr\sin^2\delta\cos\delta\,\psi_3^{(3)} + Pr^2\sin^3\delta\,\psi_4^{(3)} \\ &+ Pr\sin^3\delta\,\psi_5^{(3)} + \sin^3\delta\,\psi_6^{(3)} + \alpha_1\sin^2\delta\,\psi_7^{(3)} \\ &+ \alpha_1 Pr\sin^3\delta\,\psi_8^{(3)} + \alpha_1 Pr\sin^2\delta\cos\delta\,\psi_9^{(3)} \\ &+ \beta_1\sin^3\delta\,\psi_{10}^{(3)} + (\beta_2+\beta_3)\sin^3\delta\,\psi_{11}^{(3)}\Big], \end{aligned}$$

we recast the momentum balance (23) at this order as a set of 11 equations,

$$\nabla^2\omega_1^{(3)} = \theta_{1,x}^{(3)}, \quad \nabla^2\omega_2^{(3)} = \theta_{2,x}^{(3)} - \theta_{1,y}^{(3)},$$

$$\nabla^2\omega_3^{(3)} = \theta_{3,y}^{(3)} - 3\frac{\partial\left(\omega_1^{(1)},\psi_1^{(2)}\right)}{\partial(x,y)} - 3\frac{\partial\left(\omega_1^{(2)},\psi_1^{(1)}\right)}{\partial(x,y)},$$

$$\nabla^2\omega_4^{(3)} = -\theta_{2,y}^{(3)},$$

$$\nabla^2\omega_5^{(3)} = -\theta_{3,y}^{(3)} - 3\frac{\partial\left(\omega_1^{(1)},\psi_2^{(2)}\right)}{\partial(x,y)} - 3\frac{\partial\left(\omega_2^{(2)},\psi_1^{(1)}\right)}{\partial(x,y)},$$

$$\nabla^2\omega_6^{(3)} = -3\frac{\partial\left(\omega_1^{(1)},\psi_3^{(2)}\right)}{\partial(x,y)} - 3\frac{\partial\left(\omega_3^{(2)},\psi_1^{(1)}\right)}{\partial(x,y)},$$

$$\nabla^2\omega_7^{(3)} = -3\frac{\partial\left(\nabla^2\omega_1^{(2)},\psi_1^{(1)}\right)}{\partial(x,y)}$$

$$\nabla^2\omega_8^{(3)} = -3\frac{\partial\left(\nabla^2\omega_2^{(2)}, \psi_1^{(1)}\right)}{\partial(x,y)},$$

$$\nabla^2\omega_9^{(3)} = -3\frac{\partial\left(\nabla^2\omega_3^{(2)}, \psi_1^{(1)}\right)}{\partial(x,y)}$$

$$\nabla^2\omega_{10}^{(3)} = -6\nabla\wedge\nabla\cdot A_3^{(3)},$$

$$\nabla^2\omega_{11}^{(3)} = 6\nabla\wedge\nabla\cdot\left[tr\left(A_1^{(1)}\right)^2\underline{A}_1^{(1)}\right]$$

$$\nabla^2\psi_j^{(3)} = -\omega_j^{(3)};\quad j=1,\ldots,11.$$

The notation $\frac{\partial(\cdot,\cdot)}{\partial(x,y)}$ in these equations denotes the usual Wronskian. The solution to the sets of 3 and 11 equations for the temperature and velocity fields, respectively, are obtained by a finite difference method, where the partial derivatives are approximated by central differences. The resulting algebraic equations are solved by optimal successive over-relaxation. The optimum relaxation parameters need to be determined only once for ψ–ω set and once for an energy equation set.

2.4. Fourth-order solution for the temperature field

The effect of structural non-linearities on the temperature field is felt at the fourth order of the analysis for the first time. The problem which defines the temperature field at this order is derived from Eqs. (5) and (9),

$$\nabla^2\theta^{(4)} = Pr\left[4\frac{\partial\left(\theta^{(3)},\psi^{(1)}\right)}{\partial(x,y)} - 4\frac{\partial\left(\theta^{(1)},\psi^{(3)}\right)}{\partial(x,y)} + 6\frac{\partial\left(\theta^{(2)},\psi^{(2)}\right)}{\partial(x,y)}\right], \tag{26}$$

with homogeneous boundary conditions. For convenience we define,

$$\theta^{(4)} = G^3 Pr\Big[Pr^2\sin\delta\cos^2\delta\,\theta_1^{(4)} + Pr\sin^3\delta\cos\delta\theta_2^{(4)} + Pr\sin^2\delta\cos\delta\,\theta_3^{(4)} + Pr^2\sin^3\delta\,\theta_4^{(4)} + Pr\sin^3\delta\theta_5^{(4)} + \sin^3\delta\,\theta_6^{(4)} + \alpha_1\sin^3\delta\,\theta_7^{(4)} + \alpha_1 Pr\sin^3\delta\,\theta_8^{(4)} + \alpha_1 Pr\sin^2\delta\cos\delta\,\theta_9^{(4)} + \beta_1\sin^3\delta\,\theta_{10}^{(4)} + (\beta_2+\beta_3)\sin^3\delta\,\theta_{11}^{(4)}\Big],$$

and obtain the following set of equations from Eq. (26),

$$\nabla^2\theta_1^{(4)} = -2\psi_{1,x}^{(3)},$$

$$\nabla^2\theta_2^{(4)} = 4\frac{\partial\left(\theta_1^{(3)},\psi_1^{(1)}\right)}{\partial(x,y)} + 6\frac{\partial\left(\theta_1^{(2)},\psi_1^{(2)}\right)}{\partial(x,y)} - 2\psi_{2,x}^{(3)},$$

$$\nabla^2\theta_{(3)}^{(4)} = -2\psi_{3,x}^{(3)},$$

$$\nabla^2\theta_4^{(4)} = 4\frac{\partial\left(\theta_2^{(3)},\psi_1^{(1)}\right)}{\partial(x,y)} + 6\frac{\partial\left(\theta_1^{(2)},\psi_2^{(2)}\right)}{\partial(x,y)} - 2\psi_{4,x}^{(3)},$$

$$\nabla^2\theta_5^{(4)} = 4\frac{\partial\left(\theta_3^{(3)},\psi_1^{(1)}\right)}{\partial(x,y)} + 6\frac{\partial\left(\theta_1^{(1)},\psi_3^{(2)}\right)}{\partial(x,y)} - 2\psi_{5,x}^{(3)},$$

$$\nabla^2\theta_j^4 = -2\psi_{j,x}^{(3)};\quad j=6,\ldots,11.$$

These are solved numerically by the same method used in computing the third-order solution.

3. Discussion

The first Rivlin–Ericksen constant α_1^*, and also β_1^* which is related to α_1^*, are proportional to the first normal stress difference. All the driving terms with α_1 and β_1 at the third and fourth orders represent the influence of the first normal stress difference in shaping the field. It is easy to show that the dimensional form β_1^* of β_1 can be defined in terms of the shear relaxation modulus $G(s)$,

$$3!\beta_1^* = -\int_0^\infty s^3\frac{\mathrm{d}G}{\mathrm{d}s}\mathrm{d}s.$$

A representation for $G(s)$ rapidly decaying in time used by Siginer and Valenzuela [21] and Siginer [22], by no means unique,

$$G(s) = \frac{\mu}{\tau^k\Gamma(k)}s^{k-1}\mathrm{e}^{-s/\tau},\quad \tau = -\frac{\alpha_1^*}{k\mu},\quad 0<k<1,\ \alpha_1^*<0,$$

where τ, k and Γ are the relaxation time, power index and Gamma function, respectively, is assumed and β_1^* and β_1 are computed as,

$$\beta_1^* = \frac{\mu\tau^2}{2}k(k+1),\quad \beta_1 = \frac{k+1}{2k}\alpha_1^2. \tag{27}$$

We introduce the Weissenberg number W, a measure of the elasticity of the fluid, together with the Reynolds and Elasticity numbers Re and E,

$$W = \frac{\tau U}{D}, \quad Re = \frac{DU}{\nu}, \quad E = \frac{W}{Re},$$

where τ and U are the relaxation time and a characteristic velocity, respectively, and express Eq. (27), with the help of Eqs. $(24)_1$ and $(16)_2$ as,

$$\beta_1 = E^{\,2}\frac{k}{2}(k+1), \quad \alpha_1 = -kE.$$

The exponent (k) in the expression for the shear relaxation modulus $G(s)$ is both an enhancement factor for linear elasticity and a measure of the degree of coupling of the viscous and linearly elastic effects. We also introduce a dimensionless Shear-thinning number S defined as,

$$S = \frac{St}{Re}, \quad St = \frac{(\beta_2^* + \beta_3^*)U}{\rho D^3},$$

in terms of a characteristic velocity U. Then Eq. $(24)_2$ can be simply written as,

$$\beta_2 + \beta_3 = S < 0.$$

The elasticity number E which does not depend on the flow and stays constant with changing U governs the structure of the flow field and the heat transfer characteristics of the system to a much larger degree than the Shear-thinning number S. Depending on the aspect ratio, but not so much on the angle of inclination, the influence of the latter may even be negligible compared to the former.

To show that the series solution is good in an asymptotic sense, we consider the linear case ($E = S = 0$) and solve the field equations numerically by a finite difference method for different values of the Grashof number when the Prandtl number is fixed, that is for increasing Rayleigh numbers, and compare the series solution in terms of the Grashof number to the numerical solution for different angles of inclination and aspect ratios ranging from 1/2 to 3. We note that the perturbation parameter in the series is not really the dimensionless temperature difference ϵ, but rather the Grashof number Gr as $\epsilon^n G^{\,n} = Gr^n$ at each and every order. Comparison establishes that the series give better than qualitative results for Rayleigh numbers $Ra = 800$ ($Gr = 80$, $Pr = 10$), and $Ra = 200$ ($Gr = 200$, $Pr = 1$) for the linear case. As greater values of the Grashof number indicate larger convective effects, therefore significant deviations from the base state of conduction, we choose to do a parametric study for $Gr = 200$, $Pr = 1$ assuming with good reason that the asymptotic goodness of the series also holds in the constitutively non-linear case ($E \neq 0 \neq S$) at this Grashof and Prandtl numbers. Evidence that the asymptotic series for the non-linear case converge to a smoothly evolving solution in the neighborhood of the true solution, if not to the real solution itself is supplied by the temperature field. Up to and including third order terms in the analysis, the solution of the energy equation corresponds to the linear case and provides a good criteria when compared to the full numerical solution of the linear case. At worst, this choice will yield a roughly qualitative description of the field for a non-linear fluid with $Pr = 1$ at $Gr = 200$. $Pr = 1$ implies that momentum is diffused through viscosity at the same rate as heat is diffused through conduction in the fluid. For most non-Newtonian fluids, this may not hold true as heat is diffused at a rate at least an order of magnitude times slower than the rate of diffusion of momentum. Nevertheless, this does not preclude the existence of non-linear fluids with $Pr = 1$. Further, the behavior at $Pr = 1$ may certainly be a qualitative indication of the behavior at $Pr = 10$ at the same value of the Gr.

An inspection of the dimensional parameters embedded in the expressions for the elasticity and shear-thinning numbers E and S makes it clear that it is reasonable to adopt $E \sim 20$ and $S \sim -0.1$ as extremums of these parameters. Based on past experience [21,22], we choose $k = 0.05$ for the coupling parameter. Some comments on the solution at various orders in the asymptotic expansion are in order. At the first order, the temperature distribution is linear between the cold and hot walls and corresponds to pure conduction. This is the result of the damping effect of viscosity overcoming the buoyancy forces for small Gr. The stream function contours show a clockwise single cell flow. For smaller aspect ratios, the flow is parallel in the core region. This is in agreement with the results of Cormack et al. [10]. At this order, the solution for the temperature field is independent of the inclination, aspect ratio and Pr. On the other hand, the magnitude of the stream function $\psi^{(1)}$ depends on the inclination and Pr, but, contour plots are qualitatively unaltered with varying inclination and Pr. The results for the second-order temperature field $\theta^{(2)}$ show a strong dependence on x (see Fig. 1 for x) in contrast to $\theta^{(1)}$ which is independent of x. As in the case for $\psi^{(1)}$, only the magnitude of $\theta^{(2)}$ is affected by the inclination and Pr. The graph for $\psi^{(2)}$ shows a single cell counterclockwise flow. The circulation mode at the second order, however, is strongly dependent on the inclination and the Pr. At an angle of 90°, the flow structure may display several cells for instance, depending on the aspect ratio. For very small Pr, the flow is also multicellular.

At the second order, the constitutive structure is that of the fluid of grade two. Giesekus–Tanner theorem states that for incompressible non-Newtonian fluids, if the body forces have a potential, the velocity field is the same as that of the Newtonian fluid of the same zero shear viscosity. Non-Newtonian effects are felt only in the pressure field. But, in natural convec-

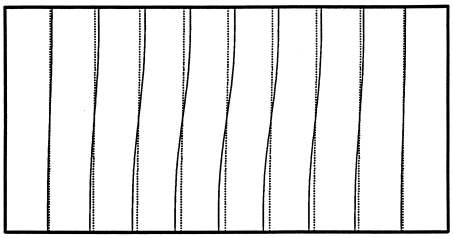

Fig. 2. Isotherms for an aspect ratio $l = 1/2$. $Gr = 200$, $Pr = 1$, $\delta = 90^\circ$, $E = 20$, $S = -0.1$. The curves represent the variation of the dimensionless temperature field θ from the hot (right) to the cold wall (left). The isotherms are equally spaced. The full and interrupted lines correspond to the non-linear ($E = 20$, $S = -0.1$) and linear ($E = S = 0$) cases, respectively.

tion, buoyant body forces do not have a potential, and it is expected in general that the velocity field of a fluid of grade two would be different from the Newtonian liquid of the same viscosity. Surprisingly, in this analysis, non-linear terms at the second order cancel out and the velocity fields are the same. Therefore, constitutive non-linearities appear in the velocity field at the third order for the first time.

Composite graphs of the velocity and temperature fields up to and including the third and fourth orders, respectively, in terms of the Grashof number will be presented for the former and the latter. Velocity fields of the linear and non-linear fluids are qualitatively similar, but velocity levels may be markedly different. Interesting phenomena are observed for aspect ratios $l \geq 1$ both in terms of the structure of the field and the heat transfer characteristics. We present in Figs. 2–5 the comparison of the isotherms for a shear-thinning and elastic fluid (full lines) and a Newtonian fluid of the same viscosity (interrupted lines) for four different aspect ratios at the same Grashof and Prandtl numbers and inclination. The isotherms do not deviate much from the linear case for $l < 1$ (Fig. 1). But as l approaches aspect ratio one from below, large devi-

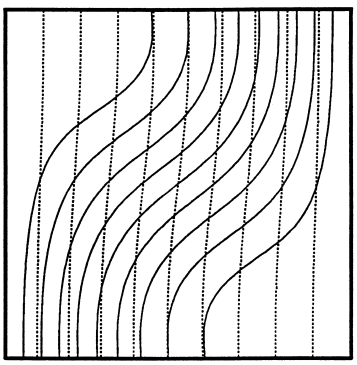

Fig. 3. Same as Fig. 2 except that the aspect ratio is $l = 1$.

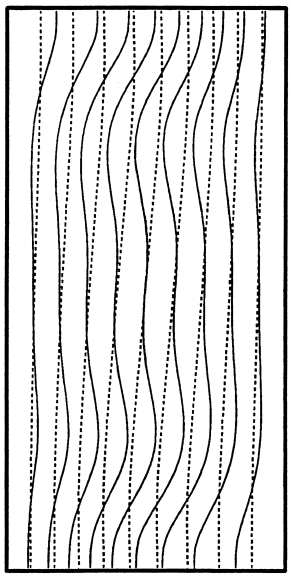

Fig. 4. Same as Fig. 2 except that the aspect ratio is $l = 2$.

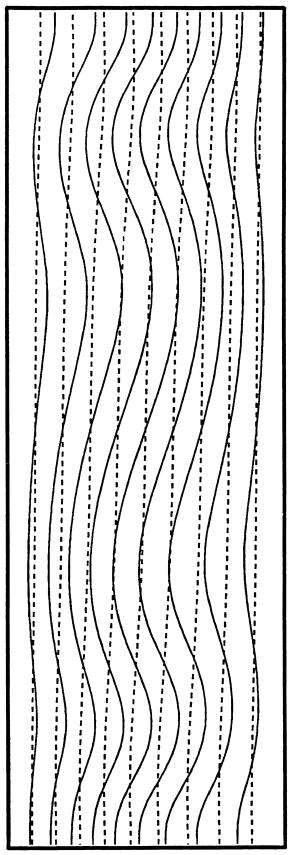

Fig. 5. Same as Fig. 2 except that the aspect ratio is $l = 3$.

ations occur (Fig. 2). At aspect ratios $l > 1$, a waviness, which tends to increase with the aspect ratio at the same Grashof number, sets in, in contrast to Newtonian isotherms which show very little of it if any (Figs. 3 and 4). The waviness may be interpreted as the onset of shear-elasticity waves, a phenomenon similar to inertial waves in steady isothermal flow, and has consequences concerning the heat transfer characteristics of the system. In particular, increasing waviness signals the imminent onset of loss of stability for the flow field.

At aspect ratios equal to and smaller than one, in a reasonably large neighborhood of $l = 1$ from below, for instance for $1/3 \leq l \leq 1$, the flow field has a single cell structure rotating in the same clockwise direction as the linear case, but the velocity levels are quite different. The cell structure remains the same as the aspect ratio $l \rightarrow 2$. But, at these large aspect ratios, the flow structure shows an interesting instability with increasing convective effects, i.e. increasing Grashof numbers, for the same values of the elasticity and shear-thinning parameters E and S (Figs. 6 and 7). The influence of increased convective effects is clear from the Newtonian plots of Figs. 6 and 7. The stream function values are increased threefold. In Fig. 6, the presence of shear-elasticity waves are signaled by the waviness of the streamlines closer to the center of the enclosure. As convective effects increase, the waviness increases and the structure of the field loses its stability, exchanging it for a multicellular structure with saddle points (Fig. 7). This loss of stability is also observed at larger aspect ratios, but it seems to occur at smaller Grashof numbers as the aspect ratio grows

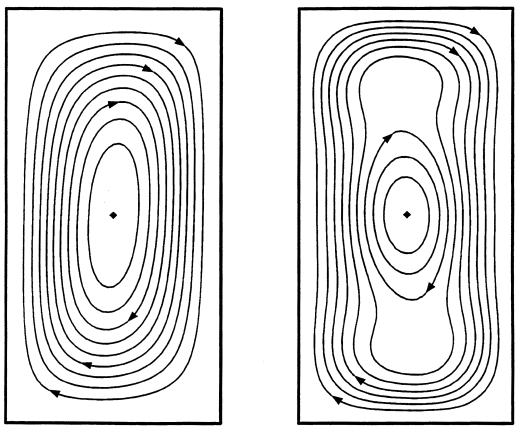

Fig. 6. Streamline contour plots for the linear (left) and nonlinear (right) cases when the aspect ratio is $l = 2$. $Gr = 85$, $Pr = 10$, $\delta = 90^\circ$, $E = 20$, $S = -0.1$, $k = 0.05$, ◆ $\psi = 0.186$ (left), ◆ $\psi = 0.178$ (right). The stream function values on the contour plots vary at equal intervals between the ψ_{max} and 0 at the walls.

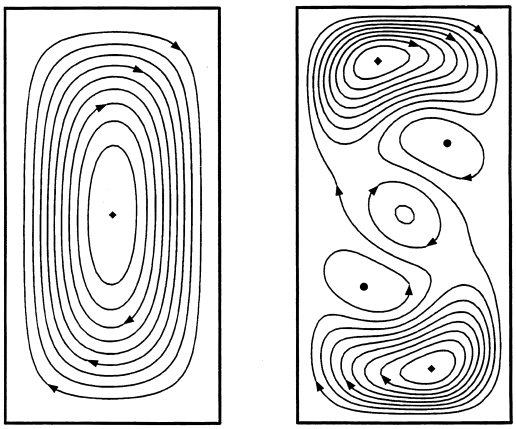

Fig. 7. Same as Fig. 6 except $Gr = 200$, $Pr = 1$, ◆ $\psi = 0.503$ (left), ◆ $\psi = 0.947$, ● $\psi = 0.113$. Streamfunction values on the contour plots vary at equal intervals between the indicated ψ's and 0 at the walls.

larger. Such behavior may lead to bubble formation and encapsulation, as is evident from Fig. 7. These features may be undesirable and are to be avoided in many industrial processes. In all the graphs presented so far, if we remove the shear-thinning capability ($S = 0$), the qualitative behavior remains the same for $l \leq 1$ and almost the same for $l > 1$. As l increases, shear-thinning effects also increase monotonically, but they are always overshadowed by elastic effects at all angles of inclination. On the other hand, removal of the elastic properties ($E = 0$) makes the field collapse to the neighborhood of the Newtonian behavior. We conclude that the elastic properties are responsible for the computed loss of stability. Very highly shear-thinning, inelastic liquids are not at all likely to show any interesting behavior qualitatively, considerably different from linear fluids. This conclusion also carries over to the heat transfer characteristics as it will be shown later. As convective effects become stronger, the instability may occur much earlier in terms of the Grashof number, all other factors being fixed, for a liquid with higher elasticity.

The variation of the average Nusselt number $\overline{Nu}$ with the inclination δ of a cavity of various aspect ratios is shown in Fig. 8. Average heat transfer as represented by $\overline{Nu}$ seems to tend towards a limit at any angle of inclination as the aspect ratio approaches 1/2 from above. The limiting value for $\overline{Nu}$ is 0.5 when $l = 1/2$. Very little variation in $\overline{Nu}$ can be detected with changing δ at this aspect ratio. For aspect ratios smaller than 1/2, there is no variation in $\overline{Nu}$ with δ. For any aspect ratio $\overline{Nu} \rightarrow 0.5$ as $\delta \rightarrow (0; \pi)$. $\overline{Nu}$ increases with increasing l, and shows considerable variation with δ, symmetric with respect to $\delta = 90^\circ$. In the absence of Bénard type instabilities, convection would

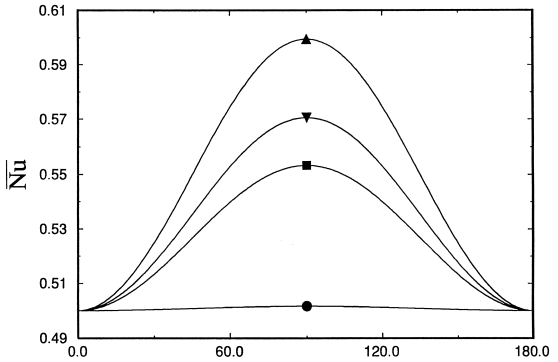

Fig. 8. Variation of the average Nusselt number $\overline{Nu}$ with aspect ratio l and angle of inclination δ. ● $l = 1/2$, ■ $l = 1$, ▲ $l = 2$, ▼ $l = 3$. $Gr = 85$, $Pr = 10$, $E = 20$, $S = -0.1$, $k = 0.05$.

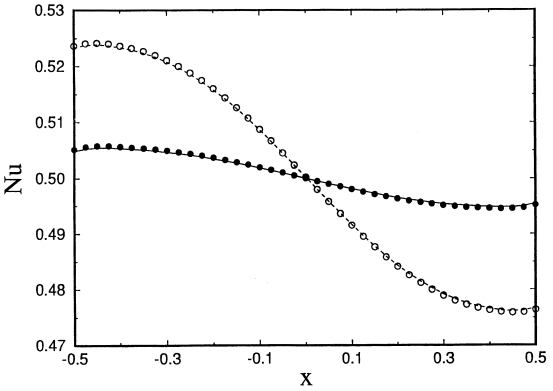

Fig. 10. Same as Fig. 9 except $\delta = 90^\circ$.

be symmetric about 90° and zero at 0 and 180°. Elasticity has very little effect on the onset of convection due to Bénard instability and the critical Rayleigh number Ra_c is almost the same as that of the linear case [19]. Thus, the $Ra = 850$ in Fig. 8 is well below Ra_c and symmetric convection and heat transfer patterns are obtained. We also note that at this Grashof and Prandtl numbers, $Gr = 85$ and $Pr = 10$, an exchange of stability has already taken place when $l = 3$, resulting in a lower $\overline{Nu}$ than when $l = 2$ at any angle of inclination.

The variation of the local Nusselt number $Nu(x)$ for different aspect ratios with changing angle of inclination shows interesting features. We present in Figs. 9 and 10 the variation of $Nu(x)$ at $\delta = 45$ and 90° when $l = 1/2$. Shear dependent viscosity characteristics have minimal influence at small aspect ratios, if at all, both in shaping the flow field and in determining the heat transfer characteristics. But, elasticity (the second normal stress difference) influences both to a large degree. This is in keeping with our previous conclusions. Heat transfer increases and decreases locally from $x = 0$ to $-L$ and from $x = 0$ to L, that is, in the lower and upper halves of the cavity, respectively, at all angles of inclination. The magnitude of this change increases with δ as $\delta \to \pi/2$ from above or below. But, interestingly enough, the increase and decrease in the lower and upper halves is almost symmetric at any δ with respect to the mid-span, and the average Nusselt number $\overline{Nu}$ is not much different from the Newtonian $\overline{Nu}$. Mid-span is approximately a fixed point which does not change with varying aspect ratio and inclination of the cavity at moderate Grashof numbers. Fig. 11 shows the variation of $Nu(x)$ for $l = 1$ at $\delta = 45^\circ$. The behavior of $Nu(x)$ when $l = 1$ and $\delta = 90^\circ$, not shown here, is similar to Fig. 11. The remarks concerning aspect ratio $l = 1/2$ remain essentially valid for $l = 1$ except local Nusselt numbers in the lower and

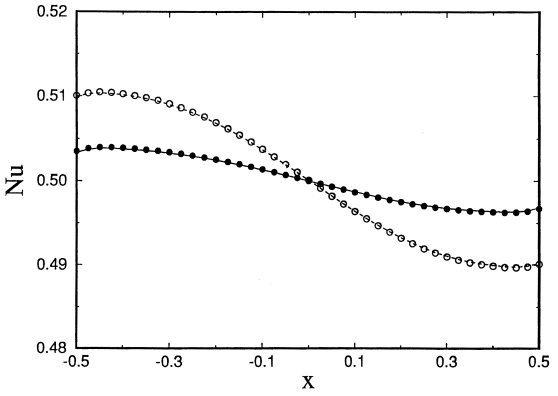

Fig. 9. Variation of the local Nusselt number $Nu(x)$ at $\delta = 45^\circ$ for $l = 1/2$. $Gr = 200$, $Pr = 1$, (—) Newtonian; (- - -) $E = 20$, $S = -0.1$, $k = 0.05$; (●) $E = 0$, $S = -0.1$; (○) E○ $= 20$, $S = 0$, $k = 0.05$.

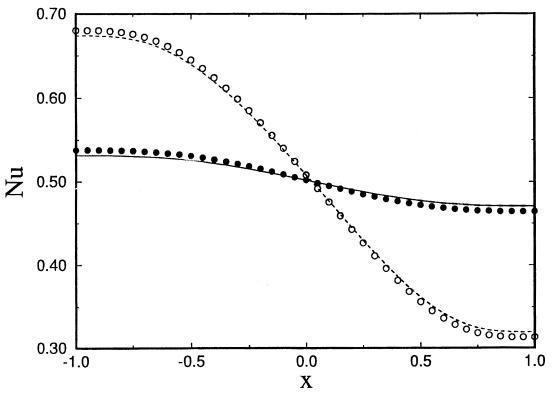

Fig. 11. Variation of the local Nusselt number $Nu(x)$ at $\delta = 45^\circ$ for $l = 1$. $Gr = 200$, $Pr = 1$, (—) Newtonian; (- - -) $E = 20$, $S = -0.1$, $k = 0.05$; (●) $E = 0$, $S = -0.1$; (○) $E = 20$, $S = 0$, $k = 0.05$.

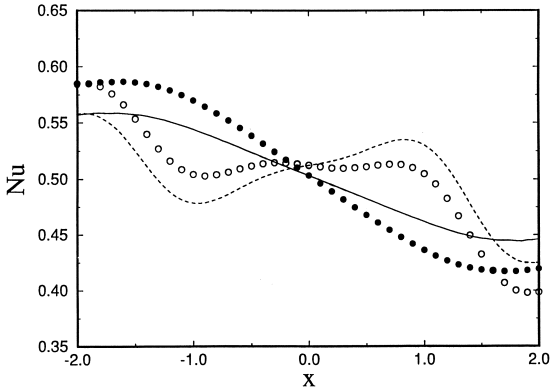

Fig. 12. Variation of the local Nusselt number $Nu(x)$ at $\delta = 45^\circ$ for $l = 2$. $Gr = 200$, $Pr = 1$, (—) Newtonian; (- - -) $E = 20$, $S = -0.1$, $k = 0.05$; (●) $E = 0$, $S = -0.1$; (○) $E = 20$, $S = 0$, $k = 0.05$.

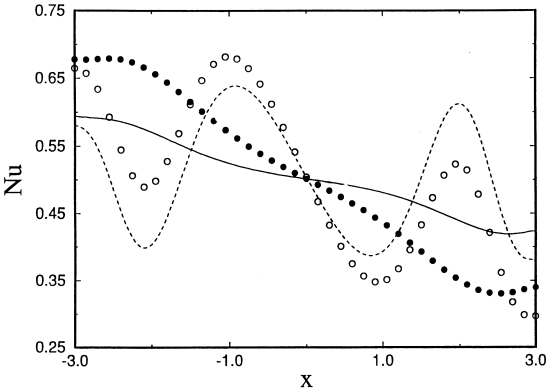

Fig. 14. Variation of the local Nusselt number $Nu(x)$ at $\delta = 90^\circ$ for $l = 3$. $Gr = 200$, $Pr = 1$, (—) Newtonian; (- - -) $E = 20$, $S = -0.1$, $k = 0.05$; (●) $E = 0$, $S = -0.1$; (○) $E = 20$, $S = 0$, $k = 0.05$.

upper halves of the cavity are much larger and smaller, respectively, than those for $l = 1/2$, in particular when $\delta = 90^\circ$. In fact, total heat transfer in the lower and upper halves of the cavity increases and decreases, respectively, monotonically at the same aspect ratio as the angle of inclination changes from 0 to 90°. Shear dependent viscosity starts making its effect felt on the field when $l = 1$. But, its influence is quite small and normal stresses always remain by far the dominant factor.

Moving on to aspect ratio $l = 2$, we present in Figs. 12 and 13 the variation of $Nu(x)$ when $\delta = 45$ and 90° after loss of stability, for the field depicted in Fig. 7 when $Gr = 200$, $Pr = 1$. The graphs of $Nu(x)$ before loss of stability for this aspect ratio are quite similar to those for $l = 1$ with the exception that overall heat transfer is higher, that is $\overline{Nu}$ is larger, and the total heat transfer together with $Nu(x)$ in the lower and upper halves of the cavity is larger and smaller, respectively. Shear thinning plays a somewhat larger role than in the case of $l = 1$. In fact, as the aspect ratio gets larger, shear-thinning effects gradually and monotonically become non-negligible in shaping the field. Shear thinning acts to attenuate somewhat elastic effects, as is evident from Figs. 10 and 11. The larger the aspect ratio and the closer the angle of inclination to 90°, the larger becomes the magnitude of this attenuation.

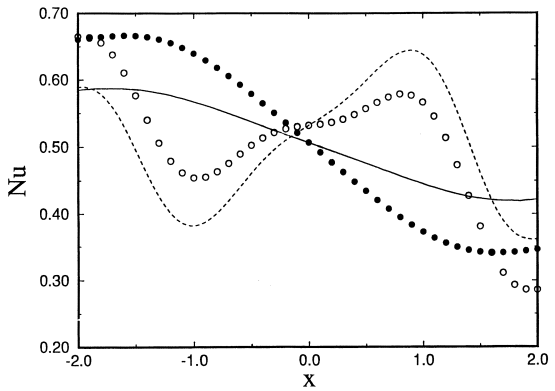

Fig. 13. Same as Fig. 12 except $\delta = 90^\circ$.

Heat transfer characteristics of the field after stability is lost and are drastically different from those of the smoothly evolving field, Figs. 12 and 13. Shear thinning is of considerable significance and enhances and lowers $\overline{Nu}$ in the lower and upper halves of the cavity, respectively, together with $Nu(x)$. But, elasticity has exactly the opposite effect, in contrast to its influence on the smoothly evolving field before the loss of stability. Increasing the angle of inclination only increases the effects of the shear thinning and of the second normal stress difference as it also did before the critical Grashof or Elasticity numbers were reached, Fig. 13. The net result is that at any angle of inclination overall heat transfer in the lower and upper halves of the cavity are lower and higher than the linear case in contrast to the comparative evolution of the non-linear case before loss of stability. The variation of $Nu(x)$ when $l = 3$ is shown in Fig. 14. Prominent features of the local heat transfer in Fig. 13 where $l = 2$ are accentuated in Fig. 14, where $l = 3$ at the same δ, thereby pointing to a clear trend as l becomes larger.

4. Conclusions

For aspect ratios smaller than one shear thinning and elastic effects through the first normal stress difference, as embodied in the dimensionless shear-thinning

and elasticity numbers, have a minimal and strong influence, respectively, in shaping the flow field and determining the heat transfer characteristics. As the aspect ratio becomes larger, their effect grows with it. The influence of shear-thinning is negligible for shallow cavities in shaping both the flow field and the heat transfer characteristics. Its influence starts becoming noticeable at $l = 1$ and gradually grows larger as the aspect ratio increases further at fixed angle of inclination and vice-versa, but always remains much smaller than normal stress effects at any angle of inclination and aspect ratio, always attenuating normal stress effects. The latter, by far the dominant factor, grow in magnitude considerably with increasing angle of inclination at fixed aspect ratio, as well as with increasing aspect ratio at fixed angle of inclination when the Grashof and Elasticity numbers are held fixed. The combined effect of shear-thinning and elasticity acts to increase and decrease total heat transfer represented by the average Nusselt number almost equally in the lower and upper halves of the cavity in the first quadrant, and vice-versa in the second, with the result that the overall heat transfer for the linear and non-linear cases are quite close at moderate Grashof numbers.

The flow fields of the Newtonian fluid and the fluid of grade three with a negative first Rivlin–Ericksen constant are qualitatively similar when both are assumed to be Boussinesq fluids and have the same zero shear viscosity. But, the velocity levels are markedly different. The flow field of the grade fluid evolves smoothly with increasing Grashof numbers at fixed Prandtl, elasticity and shear-thinning numbers until a critical Grashof number is reached. Stability is lost at gradually decreasing values of the critical Grashof number as the aspect ratio increases. The instability is triggered by the presence of elastic effects in the region of validity of the asymptotic series, and occurs at gradually higher Grashof numbers as the elasticity number is reduced at fixed aspect ratio and angle of inclination. Average and local Nusselt numbers after the loss of stability at a Grashof number close to the threshold are smaller than those at a Grashof number somewhat smaller than the critical Grashof number.

References

[1] S. Ostrach, Natural convection in enclosures, Advances in Heat Transfer 8 (1972) 161–227.

[2] B. Gebhart, Y. Jaluria, R.L. Mahajan, B. Sammakia, in: Buoyancy-Induced Flows and Transport, Hemisphere, Washington, 1988, pp. 857–890 (Chapter 16).

[3] A.V. Shenoy, Natural Convection Heat Transfer to Viscoelastic Fluids, Encyclopedia of Fluid Mechanics, in: N.P. Cheremisinoff (Ed.), Gulf, Houston, 1988.

[4] A. Emery, H.W. Chi, J.D. Dale, Free convection through vertical plane layers of non-Newtonian power law fluids, Journal of Heat Transfer 93 (1971) 164–171.

[5] K.J. Röpke, P. Schümmer, Natural convection of a viscoelastic fluid, Rheologica Acta 21 (1982) 540–542.

[6] G.K. Batchelor, Heat transfer by free convection across a closed cavity between vertical boundaries at different temperatures, Quarterly Journal of Applied Mathematics 12 (1954) 209–233.

[7] J.W. Elder, Laminar free convection in a vertical slot, Journal of Fluid Mechanics 23 (1965) 77–98.

[8] E.R.G. Eckert, W.D. Carlson, Natural convection in an air layer enclosed between two vertical plates, International Journal of Heat Mass Transfer 2 (1961) 106–120.

[9] A.E. Gill, The boundary-layer regime for convection in a rectangular cavity, Journal of Fluid Mechanics 26 (1966) 515–536.

[10] D.E. Cormack, L.G. Leal, J. Imberger, Natural convection in a shallow cavity with differentially heated end walls. Part 1. Asymptotic theory, Journal of Fluid Mechanics 65 (1974) 209–229.

[11] J. Imberger, Natural convection in a shallow cavity with differentially heated end walls. Part 3. Experimental results, Journal of Fluid Mechanics 65 (1974) 247–260.

[12] D.E. Cormack, L.G. Leal, J.H. Seinfeld, Natural convection in a shallow cavity with differentially heated end walls. Part 2. Numerical solutions, Journal of Fluid Mechanics 65 (1974) 231–246.

[13] J.O. Wilkes, S.W. Churchill, The finite difference computation of natural convection in a rectangular enclosure, American Institute of Chemical Engineers Journal 12 (1966) 161–166.

[14] G. De Vahl Davis, Laminar natural convection in an enclosed rectangular cavity, International Journal of Heat Mass Transfer 11 (1968) 1675–1693.

[15] B. Roux, J.C. Grondin, P. Bontoux, B. Gilly, On a high-order accurate method for the numerical study of natural convection in a square cavity, Numerical Heat Transfer 1 (1978) 331–349.

[16] H. Ozoe, H. Sayama, S.W. Churchill, Natural convection in an inclined square channel, International Journal of Heat Mass Transfer 17 (1974) 401–406.

[17] H. Ozoe, K. Yamamoto, H. Sayama, S.W. Churchill, Natural circulation in an inclined rectangular channel heated on one side and cooled on the opposing side, International Journal of Heat Mass Transfer 17 (1974) 1209–1217.

[18] J.N. Arnold, I. Catton, D.K. Edwards, Experimental investigation of natural convection in inclined rectangular regions of differing aspect ratios, Journal of Heat Transfer 98 (1976) 67–71.

[19] M. Sokolov, R.I. Tanner, Convective stability of a general viscoelastic fluid heated from below, The Physics of Fluids 15 (1972) 534–539.

[20] R.L. Fosdick, K.R. Rajagopal, Thermodynamics and stability of fluids of third grade, Proceedings of the Royal Society London A 339 (1980) 351–377.

[21] D.A. Siginer, A. Valenzuela-Rendón, Energy considerations in the flow enhancement of viscoelastic liquids, Journal of Applied Mechanics 60 (1993) 344–352.

[22] D.A. Siginer, On the effect of boundary vibration on Poiseuille flow of an elastico-viscous liquid, Journal of Fluids and Structures 6 (1992) 719–748.